FEBS Letters 582 (2008) 3090–3096

The crystal structure of seabream antiquitin reveals the structural basis of its substrate specificity

Wai-Kwan Tang[a], Kam-Bo Wong[a,b,*], Yuk-Man Lam[a], Sun-Shin Cha[c], Christopher H.K. Cheng[a,b], Wing-Ping Fong[a,*]

[a] *Department of Biochemistry, The Chinese University of Hong Kong, Shatin, N.T., Hong Kong, China*
[b] *Centre for Protein Science and Crystallography, The Chinese University of Hong Kong, Shatin, N.T., Hong Kong, China*
[c] *Marine Bio-Technology and New Material Research Division, Korea Ocean Research and Development Institute, Republic of Korea*

Received 28 May 2008; revised 22 July 2008; accepted 31 July 2008

Available online 9 August 2008

Edited by Hans Eklund

Abstract The crystal structure of seabream antiquitin in complex with the cofactor NAD^+ was solved at 2.8 Å resolution. The mouth of the substrate-binding pocket is guarded by two conserved residues, Glu120 and Arg300. To test the role of these two residues, we have prepared the two mutants E120A and R300A. Our model and kinetics data suggest that antiquitin's specificity towards the substrate α-aminoadipic semialdehyde is contributed mainly by Glu120 which interacts with the α-amino group of the substrate. On the other hand, Arg300 does not have any specific interaction with the α-carboxylate group of the substrate, but is important in maintaining the active site conformation.

Keywords: Antiquitin; ALDH7; α-Aminoadipic semialdehyde; X-ray crystallography; Site-directed mutagenesis; Pyridoxine-dependent epilepsy

1. Introduction

Antiquitin (ALDH7) is a member of the aldehyde dehydrogenase (ALDH) superfamily. This superfamily of enzymes is characterized by their catalytic ability to oxidize a wide variety of endogenous and exogenous aldehydes to their corresponding acids in the presence of $NAD(P)^+$ [1]. A strikingly high degree of amino acid sequence identity of ~60% has been found between plant antiquitins and their human counterpart. To reflect the "antique" nature of such a highly conserved protein, the enzyme was coined the name "antiquitin". This protein is believed to play some essential roles in certain crucial cellular processes [2,3].

In plants, antiquitin is thought to possess osmoregulatory and/or detoxification functions since expression of the enzyme is induced during dehydration [4–6]. The increase in its expression level may act to counteract the osmotic pressure changes [7] through the production of carboxylate-containing osmoprotectants and/or removal of toxic aldehydes [8]. In contrast to its plant counterparts, human antiquitin does not show any inducible response to stresses including dehydration, osmotic challenge, heat-shock and cold-shock [2,9]. Nevertheless, a change in the expression level of the enzyme could be observed during oocyte maturation in pig [10]. This, together with the observation of an increase in antiquitin level during apple fruit development [11], leads to the suggestion that antiquitin may play a developmental role.

In animals, the antiquitin protein has only been purified and characterized in fish, viz. in black seabream [8,12] and in grass carp [13]. Resembling most ALDHs, antiquitin is a homotetramer with a subunit molecular mass of ~58 kDa. Antiquitin can oxidize several aliphatic aldehydes such as acetaldehyde and propionaldehyde, but not betaine aldehyde and succinic semialdehyde [8]. However, its affinities towards these substrates are weak and hence these aldehydes are unlikely the physiological substrates of antiquitin. Recently, α-aminoadipic semialdehyde (α-AASA), an intermediate in lysine catabolism, was suggested to be the physiological substrate of antiquitin [14]. The lack of enzymatic activity of antiquitin due to mutations in the human antiquitin gene will lead to accumulation of α-AASA and its equilibrium product Δ^1-piperideine-6-carboxylate (P6C), and causes seizures in pyridoxine-dependent epilepsy patients [14,15].

Structurally, antiquitin contains all the 16 conserved amino acid residues of the ALDH superfamily [16]. Following the first crystal structure of ALDH obtained for human ALDH3 (PDB: 1AD3) [17], several structures of ALDHs have been solved, including the sheep ALDH1 (PDB: 1BXS) [18], rat retinal dehydrogenase (RALDH2) (PDB: 1BI9) [19], bovine ALDH2 (PDB: 1A4Z) [20], cod betaine aldehyde dehydrogenase (BALDH) (PDB: 1BPW) [21], *Escherichia coli* YdcW (PDB: 1WNB) [22], *Thermus thermophilus* Δ^1-pyrroline-5-carboxylate dehydrogenase (P5CDh) (PDB: 2BHQ) [23], as well as *Streptococcus mutans* non-phosphorylating glyceraldehyde-3-phosphate dehydrogenase (PDB: 2ESD) [24]. All of them exist as tetramers, except ALDH3 which is a dimeric protein. Although protein sequence alignment of these ALDHs reveals identities of less than 40%, these proteins do share a common overall folding pattern in having three discernable domains, viz. catalytic domain, NAD^+-binding domain and oligomerization domain, in each monomeric unit.

*Corresponding authors. Address: Department of Biochemistry, The Chinese University of Hong Kong, Shatin, N.T., Hong Kong, China. Fax: +852 26037732 (K.-B. Wong); fax: +852 26035123 (W.-P. Fong).
E-mail addresses: kbwong@cuhk.edu.hk (K.-B. Wong), wpfong@cuhk.edu.hk (W.-P. Fong).

Abbreviations: α-AASA, α-aminoadipic semialdehyde; ALDH, aldehyde dehydrogenase; NAD(H), nicotinamide adenine dinucleotide oxidized form (reduced form); P5CDh, Δ^1-pyrroline-5-carboxylate dehydrogenase; P6C, Δ^1-piperideine-6-carboxylate

0014-5793/$34.00
doi:10.1016/j.febslet.2008.07.059

This study reports the crystal structure of seabream antiquitin in complex with NAD^+. Based on the crystal structure of antiquitin and the accompanying mutagenesis studies, the structural basis of its substrate specificity towards α-AASA was discussed. In addition, the antiquitin structure also provides explanations for how mutations in the antiquitin gene found in pyridoxine-dependent epilepsy patients could lead to inactivation of the enzymatic activity of antiquitin.

2. Materials and methods

2.1. Crystallization, diffraction data and structure determination

Expression and purification of recombinant antiquitin in *E. coli* was performed as described previously [8]. The purified antiquitin was dissolved in 10 mM HEPES, pH 7.0, with 1 mM NAD^+ at a protein concentration of 10 mg/ml. Crystals were obtained by vapor diffusion from droplets containing 4 μl of protein solution plus 2 μl of precipitant solution containing 18% PEG 3000 and 0.1 M BIS–TRIS, pH 6.5, which were equilibrated against 1 ml of the same precipitant solution at 277 K. The crystals were loop-mounted and transferred into the cryostream at 100 K. X-ray diffraction data of the binary antiquitin-NAD^+ complex were collected using the synchrotron of beamline 6B at the Pohang Light Source, Pohang Accelerator Laboratory, Republic of Korea. The diffraction data were processed using DENZO and SCALEPACK of the HKL software [25].

The binary complex of antiquitin was solved by molecular replacement using the program MOLREP [26] in the CCP4 suite [27]. The cod BALDH (PDB: 1BPW), sharing 27% sequence identity with antiquitin, was used as the search model which was modified based on the sequence alignment [28]. The asymmetric unit contained eight monomers of antiquitin, which formed two tetramers that were in agreement with known quaternary structure of the ALDHs. Initial models were built using the program XTALVIEW [29] and refined using the program CNS [30]. To avoid model bias, model building was guided by maps generated by density-modification and composite-annealed-omit protocols, followed by refinement using the simulated annealing protocol. Eightfold non-crystallographic symmetry restraints (300 kcal mol^{-1}) were applied to all atoms of residues 8–500. The NAD^+ ligand was located with the sigma-A weighted $2mF_o–DF_c$ and $mF_o–DF_c$ maps as well as the composite-annealed-omit maps. After several rounds of refinement, REFMAC5 [31] was used for further refinement. Guided by improvement in R_{free} values, NCS restraints were extended to include residues 2–509, and the weighting was set to 'tight' for both main-chain and side-chain atoms. At this stage, 8-fold NCS-averaged maps generated by the program COOT [32] was used to guide further model rebuilding. It was later apparent that a loop (residues 329–340) of chain A adopted a conformation different from other chains, and these residues were excluded from the NCS restraints. Water molecules were located in the $F_o–F_c$ map with peaks of density >3.0σ, and only those that can form hydrogen bonds to other protein or water atoms were kept. In the final rounds of refinement, NCS restraint weighting for the side-chain atoms were reduced to 'medium' for residues 332–335, and to 'loose' for residues 9, 35, 213, 227, 248, 357, 361, 410, 499, 500, 508 and 509. Five percent of data was left out randomly for cross-validation, and the same data set was used by both CNS and REFMAC5 throughout the refinement. The final R_{free} and R_{cryst} values were 0.228 and 0.211, respectively. The small difference between R_{free} and R_{cryst} was due to the 8-fold NCS, which introduces correlation between the data in the test and working sets so that they are not completely independent of each other [33,34].

2.2. Site-directed mutagenesis

Mutations at specific sites were introduced into antiquitin by PCR using specific mutagenic primers. The sequences of the sense mutagenic primers used for generating the mutants were as follows, with the mutated codons underlined: E120A, 5′-GAGAAGTTCAGGCCTACGTTGATG-3′; R300A, 5′-AACCGCTGGCCAGGCCTGCACCA-3′. The PCR products were subcloned into pRSETA vector (Invitrogen, Carlsbad, USA). DNA sequencing was performed to confirm the sequences of the mutants. The mutants were expressed in *E. coli* BL21(DE3)LysS and purified as described for the wild-type enzyme [8].

2.3. Synthesis of P6C/α-AASA

P6C/α-AASA was synthesized as described [14]. Briefly, 10 mg allysine ethylene acetal (Chiralix B.V., Nijmegen, The Netherlands) was mixed with 40 mg Amberlyst-15 (dry) resin (Sigma–Aldrich, St. Louis, USA) in 1 ml water for 10 min. An equilibrium mixture of P6C/α-AASA was obtained from the filtrate. The amount of P6C formed was determined by reaction with 2-aminobenzaldehyde [35]. The absorbance was measured at 465 nm and an extinction coefficient of 2800 M^{-1} cm^{-1} was used for the calculation.

2.4. Determination of enzyme activity

Enzyme activity of antiquitin was measured spectrophotometrically by following the initial rate of NADH production at 340 nm in an assay medium containing 2.5 mM NAD^+ and different concentrations of the substrate. The buffers used for the substrate acetaldehyde and α-AASA were 0.1 M sodium pyrophosphate (pH 9.5) and 0.1 M MOPS (pH 7.8) [14], respectively.

3. Results and discussion

3.1. Overall structure of antiquitin

We have solved the crystal structure of seabream antiquitin in complex with NAD^+ at 2.8 Å resolution. The statistics of diffraction data and refinement are summarized in Table 1. The asymmetric unit contains two tetramers of antiquitin, each exists as a dimer-of-dimers (Fig. 1A). Each monomer is comprised of three domains, viz. NAD^+-binding domain (residues 2–132, 159–270), catalytic domain (residues 271–472), and oligomerization domain (residues 133–158, 473–511) (Fig. 1B). Such tetrameric organization of antiquitin is common in most ALDHs. The monomeric structure is also highly conserved, as shown by the low Cα rmsd (sheep ALDH1 (1.23 Å) [18], *Elephantulus edwardii* η-crystallin (1.34 Å) [36], bovine ALDH2 (1.26 Å) [20], rat ALDH3 (1.58 Å) [17], cod BALDH (1.24 Å) [21] and *E. coli* YdcW (1.22 Å) [22]).

3.2. Cofactor-binding site

The electron densities of NAD^+ are well defined and assume a single conformation (Fig. 2A). The adenosine ribose is stabilized by three hydrogen bonds: the oxygen atom AO3* interacts with the main chain oxygen of Thr163 while the side chain of Lys189 interacts with both the AO2* and AO3* atoms. The oxygen atoms of the phosphate group are hydrogen bonded with the main chain amide nitrogen as well as with the side chain hydroxyl group of Ser246. The nicotinamide ribose is stabilized by two hydrogen bonds formed between the side chain oxygens of Glu398 and the NO2* and NO3* atoms.

Two main conformations of the cofactor have been identified in different binary ALDH complexes, and isomerization between the two conformations is believed to play a crucial role in catalysis [37]. It has been proposed that bound NAD^+ prefers the "hydride-transfer" conformation where the C4 atom of the nicotinamide ring is located close to the catalytic cysteine residue ready for hydride transfer. After the transfer of hydride to the C4 atom of NAD^+, the reduced NADH isomerizes to the "hydrolysis" conformation where the nicotinamide ring is shifted towards the original position of nicotinamide ribose in the "hydride-transfer" conformation. Such displacement of the nicotinamide ring allows a water molecule to be bound and activated by the catalytic glutamine

Table 1
Summary of data collection and refinement statistics

Data statistics	
Maximum resolution (Å)	30–2.8 (2.9–2.8)
Space group	P1
Unit cell dimensions	
a, *b*, *c* (Å)	88.16, 111.023, 113.643
α, *β*, *γ* (°)	90.50, 98.10, 111.59
Temperature (K)	100
Number of measurements	246880
Number of unique reflection	86382 (7869)
Redundancy	2.9 (2.3)
Completeness (%)	93.0 (85.0)
R_{merge} [a]	0.123 (0.304)
Mean $I/\sigma(I)$	7.3 (2.1)
Refinement statistics	
R_{cryst} [b]	0.211 (0.313)
R_{free} [c]	0.228 (0.355)
Model	
Number of protein atoms	30944
Number of NAD^+ atoms	352
Number of water atoms	179
Mean *B* value (Å^2)	21.5
r.m.s. deviation from ideality	
Bond distance (Å)	0.008
Bond angles (°)	1.1
Ramachandran plot analysis [d]	
Most favored region (%)	90.9
Allowed region (%)	8.2
Generously allowed regions (%)	0.6
Disallowed regions (%)	0.2

[a] $R_{merge} = \sum_{hkl}\sum_n |I(hkl)_n - \langle I(hkl)\rangle| / \sum_{hkl}\sum_n I(hkl)_n$, where $I(hkl)_n$ is the observed intensity of the *n*th reflection and $\langle I(hkl)_n\rangle$ is the mean intensity of reflection *hkl*.
[b] $R_{cryst} = \sum^{\|} F_o| - |F_c^{\|}| / |\sum |F_o|$, where F_o and F_c are the observed and calculated amplitudes, respectively.
[c] The free set contains 4332 reflections in the structure of antiquitin-NAD^+.
[d] Ramachandran plot analysis was performed by the program PROCHECK [39].

residue (Glu267 in antiquitin) for the hydrolysis of the thioacylenzyme intermediate. Consistent with the generally accepted mechanism of ALDH, the bound NAD^+ in antiquitin is in the "hydride-transfer" conformation (Fig. 2A), and together with the catalytic Cys301, is positioned at the bottom of the funnel-shaped substrate-binding pocket (Fig. 2B).

3.3. α-AASA as the substrate of antiquitin

Using a crude cell extract as the enzyme source, α-AASA has recently been identified as a substrate of antiquitin [14]. In the present study, the oxidizing activity of antiquitin towards α-AASA was confirmed using the purified recombinant seabream enzyme with K_m and k_{cat} values of 67 μM and 6.5 s^{-1}, respectively (Table 2). The k_{cat}/K_m value of 97×10^3 M^{-1} s^{-1} is >100-fold larger than that towards the oxidation of acetaldehyde.

3.4. Site-directed mutagenesis and structural basis of substrate specificity

The substrate specificity of antiquitin towards α-AASA can be explained by the structure of the substrate-binding pocket (Fig. 2B). The lower part of the pocket is formed by hydrophobic residues such as Phe167, Ala170, Trp174 and Phe467, which are expected to form hydrophobic interactions with the aliphatic chain of α-AASA. At the mouth of the pocket, there is a pair of oppositely charged residues, Glu120 and Arg300, located ~10 Å away from each other (Fig. 2B). It is likely that they form charge-charge interactions with the α-amino and α-carboxylate groups of the substrate.

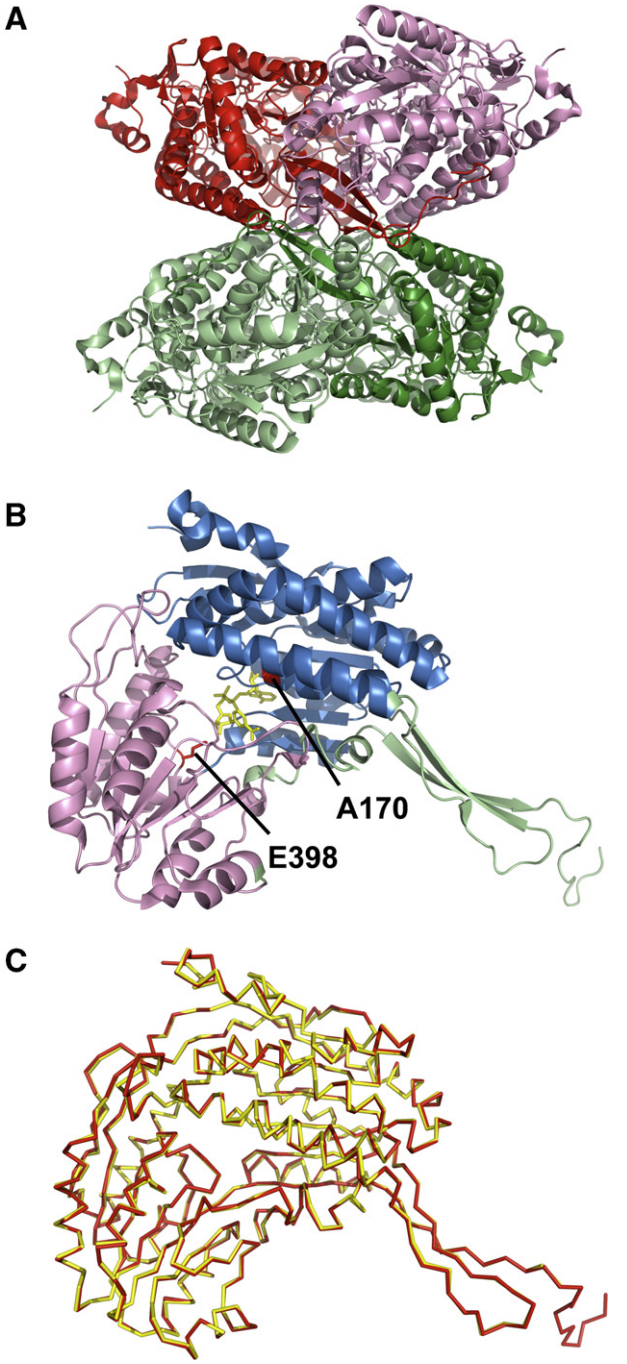

Fig. 1. (A) Tetrameric antiquitin forms a dimer-of-dimer in the crystal structure. The pale and dark green subunits form a dimer that interacts with the red and pink dimer to form an overall tetrameric structure of antiquitin. (B) Each monomer of antiquitin is consisted of a NAD^+-binding domain (blue), a catalytic domain (pink), and an oligomerization domain (green). The bound NAD^+ molecule is colored in yellow. Residues (Ala170 and Glu398) implicated in pyridoxine-dependent epilepsy are indicated in red. The figure was prepared with PyMOL (http://www.pymol.org). (C) Superimposition of Cα trace of seabream (red) and human (yellow) antiquitin.

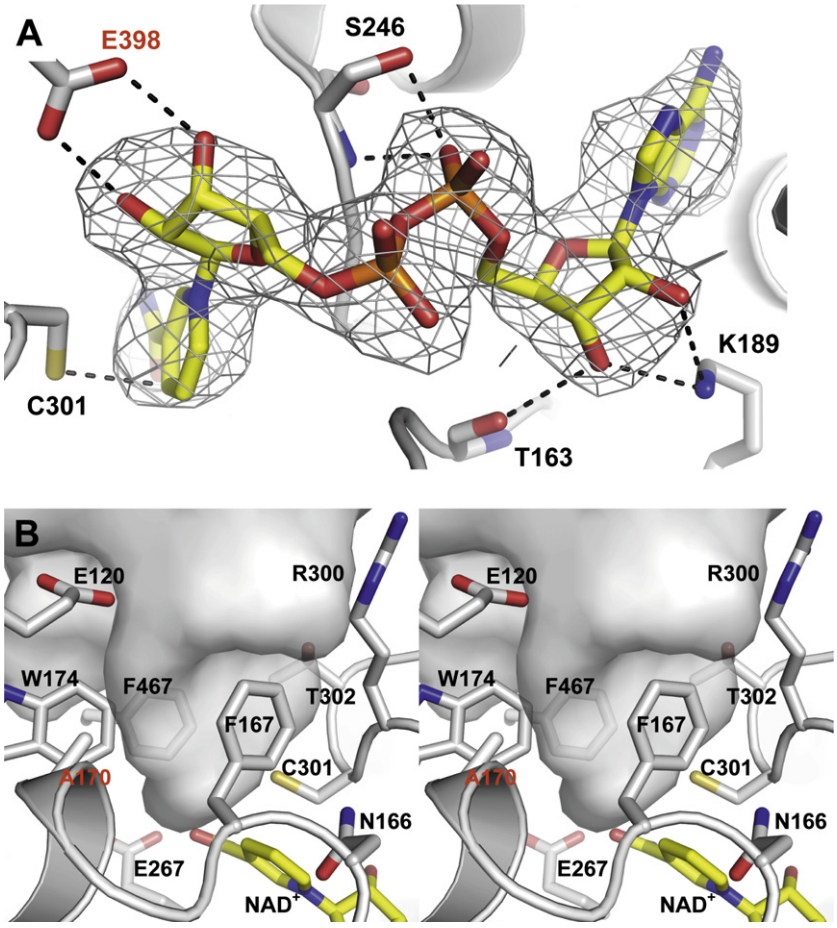

Fig. 2. (A) Bound NAD^+ in antiquitin is in a "hydride-transfer" conformation. The F_o–F_c omit electron map of NAD^+ is contoured at 3.5σ. Potential hydrogen bonds are represented in dashed lines with contacts <3 Å. The distance between the S^γ atom of Cys301 and the C4 atom of the nicotinamide ring is 3.0 Å, suggesting that the cofactor is in a "hydride-transfer" conformation. (B) Substrate-binding pocket of antiquitin. The funnel-shaped pocket is surrounded by the hydrophobic residues Phe167, Ala170, Trp174 and Phe467. The C4 atom of NAD^+ and the S^γ atom of Cys301 are pointing towards the bottom of the substrate-binding pocket, ready for the hydride-transfer reaction. The mouth of the pocket is guarded by two charged residues, Glu120 and Arg300. Residues (Ala170 and Glu398) implicated in pyridoxine-dependent epilepsy are indicated in red, and NAD^+ is in yellow in both panels. The figure was prepared with PyMOL (http://www.pymol.org).

Since these two charged residues are strictly conserved among antiquitins but not other families of ALDHs [2,4], we hypothesize that they play critical roles in determining the substrate specificity of antiquitin. To test this hypothesis, we have created two mutants, E120A and R300A of antiquitin, and measured their enzyme kinetics with α-AASA as substrate (Table 2). If the charged side chains of these residues do interact with the aldehyde substrate, alanine substitution on either of these residues will affect the α-AASA oxidizing activity of the mutants. When compared with the wild-type enzyme, the E120A substitution resulted in ~10-fold increase in the K_m value and ~8-fold decrease in the k_{cat} value (Table 2), suggesting that Glu120 is involved in stabilizing the enzyme–substrate complex through charge–charge interaction with the positively charged α-amino group of the substrate. On the other hand, the R300A substitution did not significantly alter the K_m value but resulted in ~30-fold decrease in the k_{cat} value (Table 2). These data suggest that Arg300 is not involved in substrate binding. How the mutation lower the activity of the enzyme is not clear. One possibility is that the R300A mutation removes a positively charged group that may stabilize the transition state with anionic character. Alternatively, the mutation may affect the local conformation of the adjacent catalytic residue, Cys301, thus lowering the activity of the enzyme.

The enzyme kinetics of the mutants was also studied by using acetaldehyde as substrate. The K_m values for E120A and R300A were within 4-fold of difference when compared with that of the wild-type enzyme (Table 2). Unlike α-AASA, acetaldehyde does not possess any charged side chain to have specific interaction with Glu120 at the mouth of the substrate-binding pocket. Hence, the mutation of Glu120 has a less significant effect on the binding of acetaldehyde. On the other hand, the k_{cat} value for R300A was only 2% of that for wild-type antiquitin, compared with 32 % in E120A (Table 2). Thus, for both α-AASA and acetaldehyde as substrate, Arg300 is more important than Glu120 in the catalytic process.

The site directed mutagenesis did not cause any global structural change of the enzyme, as shown from the results of circular dichroism studies. The spectra of wild-type antiquitin and the two mutants from 220 nm to 260 nm overlapped with each other with a predicted 30% helix, 10% anti-parallel, 10% parallel, 10% beta turn and 35% random coil (data not shown), showing that the activity change is a result of local conformational change.

Table 2
Kinetic parameters of antiquitin and its mutants towards the oxidation of α-AASA[a] and acetaldehyde[b]

	α-AASA			Acetaldehyde		
	K_m (μM)	k_{cat}[c] (s^{-1})	k_{cat}/K_m (M^{-1} s^{-1})	K_m (μM)	k_{cat}[c] (s^{-1})	k_{cat}/K_m (M^{-1} s^{-1})
Wild-type	67	6.5	97×10^3	3600	3.1	0.86×10^3
E120A	660	0.79	1.2×10^3	13000	1.0	0.077×10^3
R300A	52	0.22	4.2×10^3	11000	0.07	0.0064×10^3

[a]Enzymatic activities were determined in 0.1 M MOPS, pH 7.8, with 2.5 mM NAD^+ at different concentrations (0.01–1.5 mM) of α-AASA as substrate.
[b]Enzymatic activities were determined in 0.1 M sodium pyrophosphate, pH 9.5, with 2.5 mM NAD^+ at different concentrations (0.5–35 mM) of acetaldehyde as substrate.
[c]k_{cat} is calculated as NADH produced/second/active site of antiquitin.

Guided by our kinetics data and stereochemistry, we have modeled the substrate α-AASA into the active site of antiquitin (Fig. 3). Our model shows that the aliphatic chain of α-AASA fits nicely without steric clashes to the substrate-binding pocket and forms interaction with the surrounding hydrophobic residues, while the α-amino group forms a salt-bridge with Glu120. Consistent with our kinetics data, the α-carboxylate group of the substrate is not in direct contact with Arg300. The role of Arg300 is less obvious, although we believe that it is important in maintaining the overall conformation of the active site for the nucleophilic attack of Cys301 on the aldehyde carbonyl.

Both Glu120 and Arg300 are conserved among antiquitins. However, structural alignment shows that the ionic characteristics of these two residues are not conserved in other members of the ALDH superfamily. These two positions are at the entrance of the substrate-binding pocket and, in most cases, have not been shown to play any significant role in substrate binding. The different substrate-binding pockets account for the different substrate specificities of the ALDHs. For example, in *E. coli* YdcW, the positively charged trimethylammonium part of the betaine aldehyde substrate does not interact with any negatively charged amino acid residues; instead, it stacks against the phenyl ring of Phe436 and is stabilized by electrostatic interaction with the π electron cloud [22]. The substrate-binding pocket of antiquitin is most similar to that of P5CDh, an enzyme that catalyzes the oxidation of glutamate-γ-semialdehyde [23]. Glutamate-γ-semialdehyde resembles α-AASA structurally, except that the aliphatic chain in glutamate-γ-semialdehyde (5-carbon backbone) is shorter by one $–CH_2–$ unit. Although the overall amino acid sequence identity between antiquitin and P5CDh is low (~22%), the residues that form the substrate-binding pocket of the two enzymes are well conserved. A pair of charged residues, E137 and K321, corresponding to E120 and R300 respectively in antiquitin, are located at the entrance of the substrate-binding pocket of P5CDh where they stabilize the substrate through water-mediated hydrogen bonds [23]. Compared with the structure of P5CDh, the substrate-binding pocket of antiquitin is deeper and narrower. The Trp174 that forms part of the hydrophobic binding pocket of antiquitin is replaced by a glycine in P5CDh. As a result of the presence of Trp174, the carboxylate group of Glu120 in antiquitin is positioned ~3 Å above its corresponding residue (Glu137) in P5CDh. Our modeling suggests that such structural changes provide better interaction with the longer substrate α-AASA.

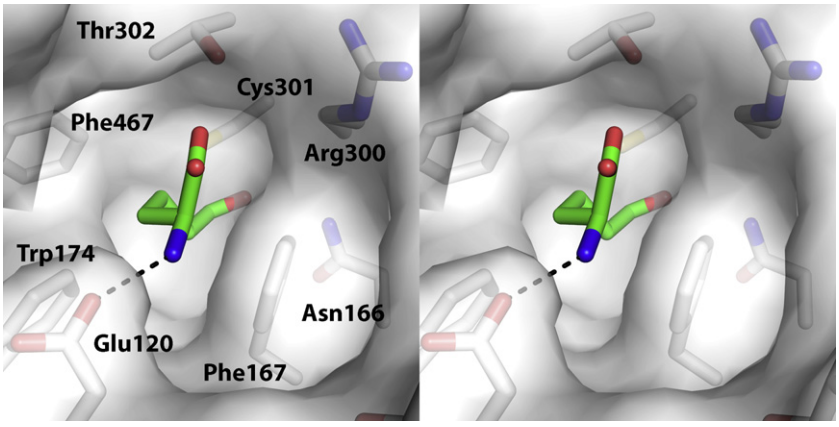

Fig. 3. Modeled structure of the enzyme–substrate complex. α-AASA was modeled into the substrate binding pocket manually using the program XTALVIEW [29]. The aldehyde function group was positioned in such a way that it forms a hydrogen bond with the backbone amide of Cys301, and allows a nucleophilic attack from the thiol group of Cys301. The torsion angles along the aliphatic chain were then adjusted to avoid steric clashes with other protein atoms in the binding pocket. Guided by our kinetics data, the α-amino group of α-AASA was positioned to form a hydrogen bond with the carboxylate group of Glu120.

3.5. Comparison with human antiquitin

During the course of this study, the structure of human antiquitin (also known as aminoadipate semialdehyde dehydrogenase, ALDH7A1) was deposited in the protein database (PDB: 2J6L). Both the monomeric and quaternary structures of seabream and human antiquitin are highly conserved. The structure of seabream antiquitin is superimposable with the human homolog, with a Cα rmsd value of 0.36 Å (Fig. 1C). The residues responsible for cofactor and substrate binding (Fig. 2) are conserved, and the conformations of these active sites residues (including Ala170 and Glu398 that are implicated in pyridoxine-dependent epilepsy, see below) are essentially identical in both seabream and human antiquitins. Based on the structural similarity (84% sequence identity) between the two homologous proteins, we believe that the model of substrate–enzyme interaction we proposed is also generally applicable to the human enzyme.

3.6. Implication in pyridoxine-dependent epilepsy

Recently, it has been found that pyridoxine-dependent epilepsy is caused by mutations in the human antiquitin (ALDH7A1) gene [14,15] that is involved in the pipecolic acid pathway of lysine degradation. Mutations that inactivate the enzyme will lead to the accumulation of α-AASA and P6C. P6C condenses with and depletes pyridoxal phosphate, an essential cofactor in amino acid and neurotransmitter metabolism; subsequently leading to seizures in the patients. Two point-mutations, E399Q and A171V, in human antiquitin that result in a decrease or a complete absence of oxidizing activity towards α-AASA were identified [14,15].

The structural mechanism of enzyme inactivation by these two mutations can be explained by the crystal structures of antiquitin. E399Q is a common mutation in pyridoxine-dependent epilepsy patients. In a recent study, it has been identified in 12 of 36 alleles in a cohort of 18 patients [14,15]. This glutamate residue (Glu398 in seabream antiquitin) is involved in binding NAD^+ by forming hydrogen bond with the nicotinamide ribose (Fig. 2A). Substitution of this charged amino acid by the polar glutamine residue in the human E399Q antiquitin mutant will disturb its interaction with the cofactor and result in a decrease in enzyme activity. Noteworthy, this glutamate residue is conserved among the ALDH superfamily, and the effect of a glutamine substitution at this position has been previously demonstrated in human ALDH2 [38]. On the other hand, Ala171 (Ala170 in seabream antiquitin) forms part of the substrate-binding pocket (Fig. 2B). Substitution with a bulky amino acid such as valine (A171V) at this position will result in steric clashes with surrounding residues in the substrate-binding pocket (e.g. Glu120, Phe167, Trp174), leading to a loss in catalytic activity.

3.7. Concluding remarks

In summary, we have solved the crystal structure of seabream antiquitin in complex with NAD^+ at 2.8 Å resolution, which provides the structural basis of substrate specificity towards α-AASA. Confirmed by site-directed mutagenesis, two conserved residues, Glu120 and Arg300 located at the mouth of the substrate-binding pocket, were found to play crucial role in enzyme catalysis of antiquitin. Glu120 is more important for substrate specificity while Arg300 is critical for catalytic activity. To further prove the roles of these two amino acid residues, crystallographic studies of the ternary complex of antiquitin (and its mutants) with NAD^+ and substrate analog are in progress. The structure of antiquitin also provides valuable insights into how mutations found in pyridoxine-dependent epilepsy patients inactivate the enzymatic activity of antiquitin.

Note

The atomic coordinates and structure factors of the binary complex of seabream antiquitin with NAD^+ (PDB: 2JG7) have been deposited in the Protein Data Bank, Research Collaboratory for Structural Bioinformatics, Rutgers University, New Brunswick, NJ (http://www.rcsb.org/).

Acknowledgements: This work was supported by a grant from the Research Grants Council of the Hong Kong Special Administrative Region (Project No. 464407). Work performed at KORDI was supported by the Marine & Extreme Genome Research Center Program, Ministry of Land, Transport, and Maritime Affairs, Republic of Korea.

References

[1] Sophos, N.A., Black, W.J. and Vasiliou, V. (2006) An update of the ALDH gene family (Weiner, H., Plapp, B., Lindahl, R. and Maser, E., Eds.), Enzymology and Molecular Biology of Carbonyl Metabolism, Vol. 12, pp. 3–7, Purdue University Press, Indiana.

[2] Lee, P., Kuhl, W., Gelbart, T., Kamimura, T., West, C. and Beutler, E. (1994) Homology between a human protein and a protein of the green garden pea. Genomics 21, 371–378.

[3] Fong, W.P., Cheng, C.H.K. and Tang, W.K. (2006) Antiquitin, a relatively unexplored member in the superfamily of aldehyde dehydrogenases with diversified physiological functions. Cell. Mol. Life Sci. 63, 2881–2885.

[4] Guerrero, F.D., Jones, J.T. and Mullet, J.E. (1990) Turgor-responsive gene transcription and RNA levels increase rapidly when pea shoots are wilted. Sequence and expression of three inducible genes. Plant Mol. Biol. 15, 11–26.

[5] Stroeher, V.L., Boothe, J.G. and Good, A.G. (1995) Molecular cloning and expression of a turgor-responsive gene in *Brassica napus*. Plant Mol. Biol. 27, 541–551.

[6] Kirch, H.H., Schlingensiepen, S., Kotchoni, S., Sunkar, R. and Bartels, D. (2005) Detailed expression analysis of selected genes of the aldehyde dehydrogenase (ALDH) gene superfamily in *Arabidopsis thaliana*. Plant Mol. Biol. 57, 315–332.

[7] Rodrigues, S.M., Andrade, M.O., Gomes, A.P., Damatta, F.M., Baracat-Pereira, M.C. and Fontes, E.P. (2006) Arabidopsis and tobacco plants ectopically expressing the soybean antiquitin-like ALDH7 gene display enhanced tolerance to drought, salinity, and oxidative stress. J. Exp. Bot. 57, 1909–1918.

[8] Tang, W.K., Chan, C.B., Cheng, C.H.K. and Fong, W.P. (2005) Seabream antiquitin: molecular cloning, tissue distribution, subcellular localization and functional expression. FEBS Lett. 579, 3759–3764.

[9] Wong, W.Y., Cheng, C.H.K. and Fong, W.P. (2006) Lack of inducibility of antiquitin (ALDH7A1) in cultured human embryonic kidney (HEK293) cell under osmotic or oxidative stress (Weiner, H., Plapp, B., Lindahl, R. and Maser, E., Eds.), Enzymology and Molecular Biology of Carbonyl Metabolism, Vol. 12, pp. 96–103, Purdue University Press, Indiana.

[10] Ellederova, Z., Halada, P., Man, P., Kubelka, M., Motlik, J. and Kovarova, H. (2004) Protein patterns of pig oocytes during *in vitro* maturation. Biol. Reprod. 71, 1533–1539.

[11] Yamada, K., Mori, H. and Yamaki, S. (1999) Identification and cDNA cloning of a protein abundantly expressed during apple fruit development. Plant Cell Physiol. 40, 198–204.

[12] Tang, W.K., Cheng, C.H.K. and Fong, W.P. (2002) First purification of the antiquitin protein and demonstration of its enzymatic activity. FEBS Lett. 516, 183–186.
[13] Chan, W.M., Tang, W.K., Cheng, C.H.K. and Fong, W.P. (2003) Purification, N-terminal sequence determination and enzymatic characterization of antiquitin from the liver of grass carp. Comp. Biochem. Physiol. B Biochem. Mol. Biol. 136, 443–450.
[14] Mills, P.B. et al. (2006) Mutations in antiquitin in individuals with pyridoxine-dependent seizures. Nat. Med. 12, 307–309.
[15] Plecko, B. et al. (2007) Biochemical and molecular characterization of 18 patients with pyridoxine-dependent epilepsy and mutations of the antiquitin (ALDH7A1) gene. Hum. Mutat. 28, 19–26.
[16] Perozich, J., Nicholas, H., Wang, B.C., Lindahl, R. and Hempel, J. (1999) Relationships within the aldehyde dehydrogenase extended family. Protein Sci. 8, 137–146.
[17] Liu, Z.J. et al. (1997) The first structure of an aldehyde dehydrogenase reveals novel interactions between NAD and the Rossmann fold. Nat. Struct. Biol. 4, 317–326.
[18] Moore, S.A., Baker, H.M., Blythe, T.J., Kitson, K.E., Kitson, T.M. and Baker, E.N. (1998) Sheep liver cytosolic aldehyde dehydrogenase: the structure reveals the basis for the retinal specificity of class 1 aldehyde dehydrogenases. Structure 6, 1541–1551.
[19] Lamb, A.L. and Newcomer, M.E. (1999) The structure of retinal dehydrogenase type II at 2.7 Å resolution: implications for retinal specificity. Biochemistry 38, 6003–6011.
[20] Steinmetz, C.G., Xie, P., Weiner, H. and Hurley, T.D. (1997) Structure of mitochondrial aldehyde dehydrogenase: the genetic component of ethanol aversion. Structure 5, 701–711.
[21] Johansson, K., El-Ahmad, M., Ramaswamy, S., Hjelmqvist, L., Jornvall, H. and Eklund, H. (1998) Structure of betaine aldehyde dehydrogenase at 2.1 Å resolution. Protein Sci. 7, 2106–2117.
[22] Gruez, A., Roig-Zamboni, V., Grisel, S., Salomoni, A., Valencia, C., Campanacci, V., Tegoni, M. and Cambillau, C. (2004) Crystal structure and kinetics identify *Escherichia coli* YdcW gene product as a medium-chain aldehyde dehydrogenase. J. Mol. Biol. 343, 29–41.
[23] Inagaki, E., Ohshima, N., Takahashi, H., Kuroishi, C., Yokoyama, S. and Tahirov, T. (2006) Crystal structure of *Thermus thermophilus* delta(1)-pyrroline-5-carboxylate dehydrogenase. J. Mol. Biol. 362, 490–501.
[24] D'Ambrosio, K., Pailot, A., Talfournier, F., Didierjean, C., Benedetti, E., Aubry, A., Branlant, G. and Corbier, C. (2006) The first crystal structure of a thioacylenzyme intermediate in the ALDH family: new coenzyme conformation and relevance to catalysis. Biochemistry 45, 2978–2986.
[25] Otwinowski, Z. and Minor, W. (1997) Processing of X-ray diffraction data collected in oscillation mode. Meth. Enzymol. 276, 307–326.
[26] Vagin, A.A. and Isupov, M.N. (2001) Spherically averaged phased translation function and its application to the search for molecules and fragments in electron-density maps. Acta Crystallogr. D Biol. Crystallogr. 57, 1451–1456.
[27] Collaborative Computational Project, N. (1994) The CCP4 suite: programs for protein crystallography. Acta Crystallogr. D Biol. Crystallogr. 50, 760–763.
[28] Cheung, Y.Y., Allen, M.D., Bycroft, M. and Wong, K.B. (2004) Crystallization and preliminary crystallographic analysis of an acylphosphatase from the hyperthermophilic archaeon *Pyrococcus horikoshii*. Acta Crystallogr. D Biol. Crystallogr. 60, 1308–1310.
[29] McRee, D.E. (1999) XtalView/Xfit—a versatile program for manipulating atomic coordinates and electron density. J. Struct. Biol. 125, 156–165.
[30] Brunger, A.T. et al. (1998) Crystallography & NMR system: a new software suite for macromolecular structure determination. Acta Crystallogr. D Biol. Crystallogr. 54, 905–921.
[31] Murshudov, G.N., Vagin, A.A. and Dodson, E.J. (1997) Refinement of macromolecular structures by the maximum-likelihood method. Acta Crystallogr. D Biol. Crystallogr. 53, 240–255.
[32] Emsley, P. and Cowtan, K. (2004) Coot: model-building tools for molecular graphics. Acta Crystallogr. D Biol. Crystallogr. 60, 2126–2132.
[33] Kleywegt, G.J. and Brünger, A.T. (1996) Checking your imagination: applications of the free *R* value. Structure 4, 897–904.
[34] Fabiola, F., Korostelev, A. and Chapman, M.S. (2006) Bias in cross-validated free *R* factors: mitigation of the effects of non-crystallographic symmetry. Acta Crystallogr. D Biol. Crystallogr. 62, 227–238.
[35] Soda, K., Misono, H. and Yamamoto, T. (1968) L-Lysine:alpha-ketoglutarate aminotransferase. I. Identification of a product, delta-1-piperideine-6-carboxylic acid. Biochemistry 7, 4102–4109.
[36] Bateman, O.A., Purkiss, A.G., van Montfort, R., Slingsby, C., Graham, C. and Wistow, G. (2003) Crystal structure of eta-crystallin: adaptation of a class 1 aldehyde dehydrogenase for a new role in the eye lens. Biochemistry 42, 4349–4356.
[37] Perez-Miller, S.J. and Hurley, T.D. (2003) Coenzyme isomerization is integral to catalysis in aldehyde dehydrogenase. Biochemistry 42, 7100–7109.
[38] Ni, L., Sheikh, S. and Weiner, H. (1997) Involvement of glutamate 399 and lysine 192 in the mechanism of human liver mitochondrial aldehyde dehydrogenase. J. Biol. Chem. 272, 18823–18826.
[39] Laskowski, R.A., MacArthur, M.W., Moss, D.S. and Thornton, J.M. (1993) PROCHECK: a program to check the stereochemical quality of protein structures. J. Appl. Crystallogr. 26, 283–291.